International Journal of Heat and Mass Transfer 163 (2020) 120393

Contents lists available at ScienceDirect

International Journal of Heat and Mass Transfer

journal homepage: www.elsevier.com/locate/hmt

Remarkably reduced thermal contact resistance of graphene/olefin block copolymer/paraffin form stable phase change thermal interface material

Changqing Liu[a,b], Wei Yu[c,*], Cheng Chen[c], Huaqing Xie[c], Bingyang Cao[d,*]

[a] School of Mechanical and Energy Engineering, Shaoyang University, Shaoyang 422000, China
[b] Key Laboratory of Hunan Province for Efficient Power System and Intelligent Manufacturing, Shaoyang University, Shaoyang 422000, China
[c] College of Engineering, Shanghai Key Laboratory of Engineering Materials Application and Evaluation, Shanghai Polytechnic University, Shanghai 201209, China
[d] Key Laboratory for Thermal Science and Power Engineering of Ministry of Education, Department of Engineering Mechanics, Tsinghua University, Beijing 100084, China

ARTICLE INFO

Article history:
Received 15 April 2020
Revised 19 August 2020
Accepted 23 August 2020

Keywords:
Thermal contact resistance
Thermal conductivity
Phase change
Thermal interface materials
Critical thickness
Graphene

ABSTRACT

Thermal contact resistance is a key bottleneck to restrict the rapid heat dissipation of electronic device. The wetting between two contact surfaces is one of the most important factors affecting the thermal contact resistance. Phase change thermal interface material can transform from solid state to molten state by heat inducing, which is an efficient way to reduce the thermal contact resistance. In this work, a novel form stable phase change thermal interface material of graphene/olefin block copolymer/paraffin filled with graphene (≤4.0 wt%) was designed. Furthermore, the influence of temperature and pressure on thermal contact resistance were studied, and the dominant position of thermal contact resistance and R_{TIMs} in total thermal resistance was analyzed systematically. The results exhibit that thermal contact resistance decreases sharply from 8–20 Kcm^2/W to 0.1–0.2 Kcm^2/W for the temperature increases from 37 °C to 45 °C (50 Psi), with a drop of up to two orders of magnitude. This is because the wettability of the two contact surfaces is greatly improved by changing solid–liquid contact to solid–liquid contact. In addition, the thermal contact resistance decreases slightly with the increase of pressure (10–50 Psi, 48 °C). A small amount of graphene can significantly enhance the thermal conductivity of graphene/olefin block copolymer/paraffin, but the effect on thermal contact resistance is relatively weak. Moreover, critical thickness is proposed to quantitatively evaluate the dominant position of thermal contact resistance or R_{TIMs} in total thermal resistance. It facilitates the quantitative analysis and optimization of thermal resistance in practical application.

1. Introduction

Poor heat dissipation has become one of the main bottlenecks restricting the further development of microelectronics industry [1–3]. Fortunately, thermal interface materials (TIMs) are used to connect radiator and heat source, which is an efficient approach to solve the heat dissipation problem of microelectronic products [4–6]. For the whole heat transfer process, there are three parts of thermal resistance related to the TIMs, the thermal resistance of TIMs itself (R_{TIMs}), and the thermal contact resistance (TCR) between TIMs and two contact surfaces (Fig. 1(a) and (b)) [7–11]. Until now, there have been many methods to enhance the thermal conductivity of TIMs (decrease of R_{TIMs}) and significant progress have been achieved, such as filling with high thermal conductivity additives [12–15], constructing efficient heat conduction network chain in matrix [16–19], or strengthening the interaction between filler and matrix [20–23]. In addition, TCR is also an important component in total thermal resistance, but theoretical and experimental studies on the TCR are rare. Especially when the thickness of TIMs is thin and the thermal conductivity of TIMs is high (the ultimate goal of TIMs in practical application), TCR will play a dominant role in the total thermal resistance. Therefore, it is urgent to explore the influencing factors of TCR through experiments, and provide a feasible scheme to reduce TCR.

TCR is mainly affected by temperature, pressure and wettability between two contact surfaces [24,25]. It will be a perfect thing to find a TIMs easy to use and with low TCR. Luckily, phase change thermal interface materials (Ph-TIMs) fully meet these require-

* Corresponding authors
E-mail addresses: yuwei@sspu.edu.cn (W. Yu), caoby@tsinghua.edu.cn (B. Cao).

https://doi.org/10.1016/j.ijheatmasstransfer.2020.120393
0017-9310/

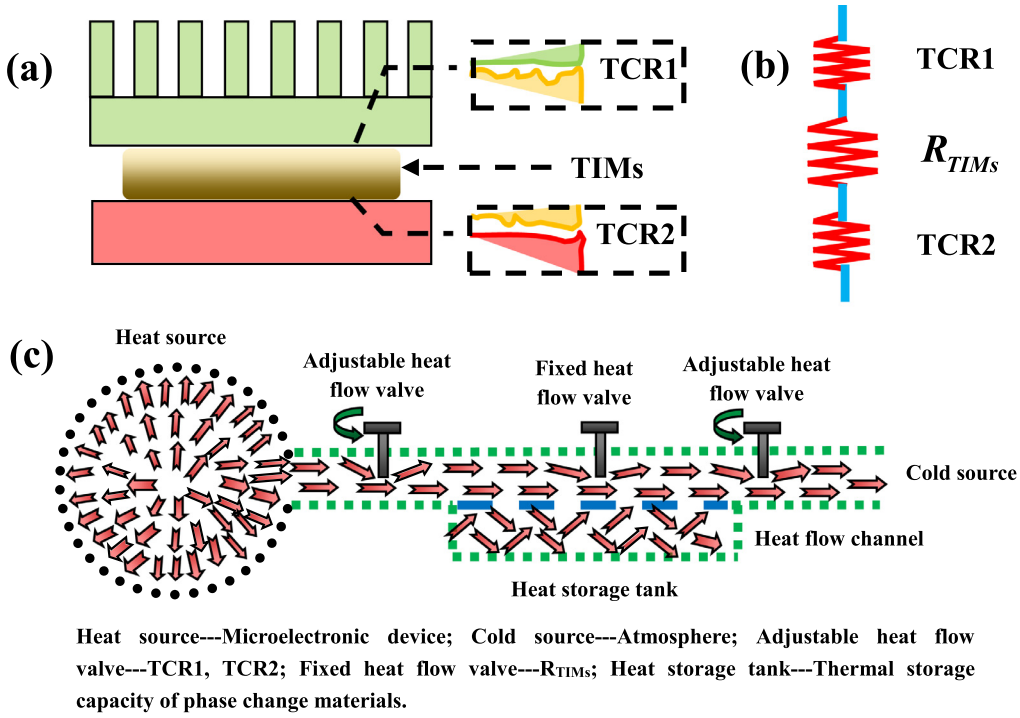

Fig. 1. Schematic diagram for (a) TIMs are applied to heat dissipation of microelectronic device; (b) total thermal resistance distribution of based on TIMs; and (c) working principle of Ph-TIMs.

ments and are easy to use. Ph-TIMs is in solid state when it is not in working state. When it is in working state, it gradually changes from solid state to molten state, which greatly improves the wettability between Ph-TIMs and heat source or radiator, and reduces the TCR. The schematic diagram for working principle of Ph-TIMs is proposed in Fig. 1(c). It mainly includes heat source (microelectronic products), cold source (atmosphere), heat flow channel, adjustable heat flow valve (TCR), fixed heat flow valve (R_{TIMs}) and heat storage tank (thermal storage capacity of phase change materials). When the microelectronic devices work, they will produce a lot of heat, so their temperature will rise continuously (heat source), and the temperature of Ph-TIMs, which is in close contact with them, will also continue to enhance. The Ph-TIMs gradually change from solid state to molten state, and the contact between Ph-TIMs and heat source will change from solid–solid contact to solid–liquid contact. Moreover, the TCR is greatly reduced. As the opening of the adjustable heat flow valve is increased, the heat flow transportation is accelerated. Therefore, the temperature of heat source is prevented from further rising, and finally the system reaches a new stable state, and the heat source maintains a lower working temperature. The final equilibrium temperature of microelectronic devices depends on the heat generation rate and the total thermal resistance.

Paraffin (PA) is one of the most common organic phase change materials. It shows a lot of excellent properties, such as higher latent heat, lower melting temperature and chemical stability [26–28]. The phase change temperature of PA (about 40–50 °C) is lower than the maximum temperature allowed by the normal operation of microelectronic device. However, it has the disadvantages of low thermal conductivity and being easy to leak. Graphene is a new type of two-dimensional layered nano material with high thermal conductivity, which is an excellent additive used to enhance the thermal transport properties of other matrix materials. In addition, olefin block copolymer (OBC) is a novel heat induced elastomer multi-block copolymer, which is produced from Dow Chemical Company by using chain shutting technology. It can be used to prevent the leakage of phase change materials in the process of phase change and to maintain the even distribution of graphene in PA matrix due to unique structural characteristics [28].

In our previous research, we designed one kind of Ph-TIMs of Al_2O_3/OBC/PA at large loading (10–80 wt%) [29]. It confirmed that TCR increases with the addition of Al_2O_3 increases. Adding more solid additives increased the viscosity of the composite and weakened the wetting between the two contact surfaces. Therefore, it suggested that Ph-TIMs of G/OBC/PA filled with a small amount of high conductivity graphene will show very low TCR. Meanwhile, it is also very important to evaluate TCR and R_{TIMs} which are dominant in the total thermal resistance.

In this work, based on the complementary relationship among the excellent properties of graphene, PA and OBC, a novel Ph-TIMs of G/OBC/PA with low thermal contact resistance, high thermal conductivity and form-stable shape is proposed. Firstly, the influence of temperature and pressure on TCR are studied. Secondly, the influence of the amount of additives on the TCR of OBC/PA is explored. Finally, A method to evaluate the dominant position of TCR and R_{TIMs} in total thermal resistance is supplied. A remarkably reduced thermal contact resistance of graphene/olefin block copolymer/paraffin is obtained, which provides valuable reference for the future practical application.

2. Experimental section

2.1. Materials

The main raw materials involved in the experiment were OBC, PA and graphene. OBC (Commercial grade 9530) with heat induced elasticity was supplied by Dow Chemical Co., Ltd. PA (OP44E) with phase change temperature range of 41–44 °C was obtained from Hangzhou Ruhr Energy Technology Co., Ltd. The thermal conductivity of PA was 0.2 *W/mK*. Graphene was supplied by Shanghai Xihan New Materials Co., Ltd.

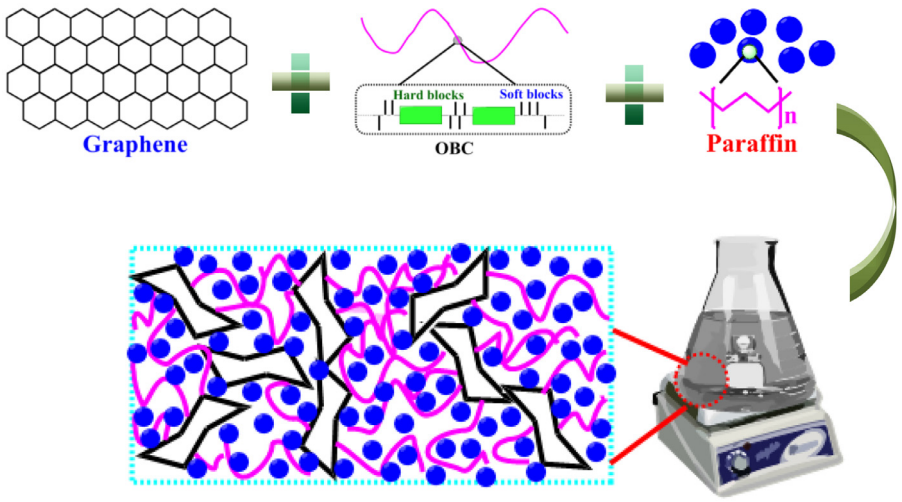

Fig. 2. Schematic diagram for preparation process of G/OBC/PA.

Table 1
Detailed quantity of components in different Ph-TIMs.

Sample	PA (g)	OBC (g)	Graphene (wt%)	Remarks (abbreviated)
1	2.00	0.50	0	S_0
2	2.00	0.50	0.1	$S_{0.1}$
3	2.00	0.50	0.5	$S_{0.5}$
4	2.00	0.50	1.0	$S_{1.0}$
5	2.00	0.50	1.5	$S_{1.5}$
6	2.00	0.50	2.0	$S_{2.0}$
7	2.00	0.50	2.5	$S_{2.5}$
8	2.00	0.50	3.0	$S_{3.0}$
9	2.00	0.50	3.5	$S_{3.5}$
10	2.00	0.50	4.0	$S_{4.0}$

2.2. Preparation

The preparation process for PA based Ph-TIMs filled with different mass fraction of graphene were as follows: 2 g PA was added to the beaker and heated to 60 °C. When the PA was completely melted, graphene (detailed quantities of additives are shown in Table 1.) was added and stirred thoroughly (magnetic stirring, 500 rpm, 60 mins). The mixture was then gradually heated to 160 °C and 0.5 g OBC was slowly added (PA:OBC=8:2). The mass ratio of PA to OBC came from literature 28. When the mixture got well dispersed and uniform, it was poured into the stainless steel mould to cool down and form. The preparation process of G/OBC/PA was shown in Fig. 2.

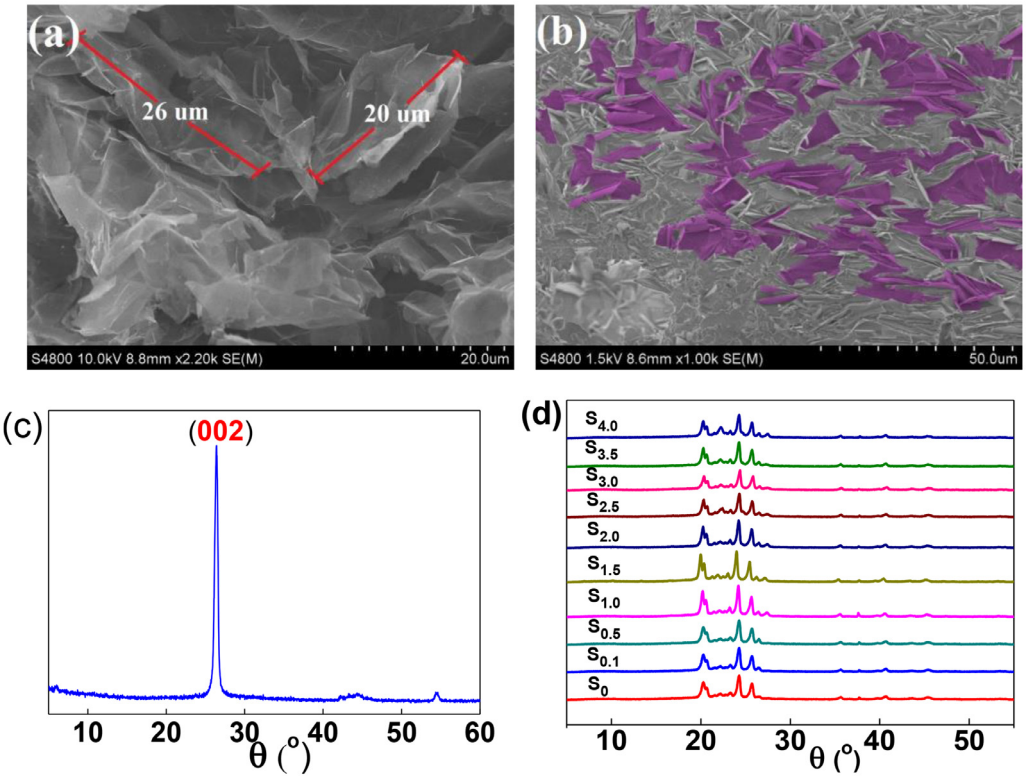

Fig. 3. SEM images of (a) graphene, (b) cross section of $S_{2.0}$; and XRD results of (c) graphene, (d) S_0–$S_{4.0}$.

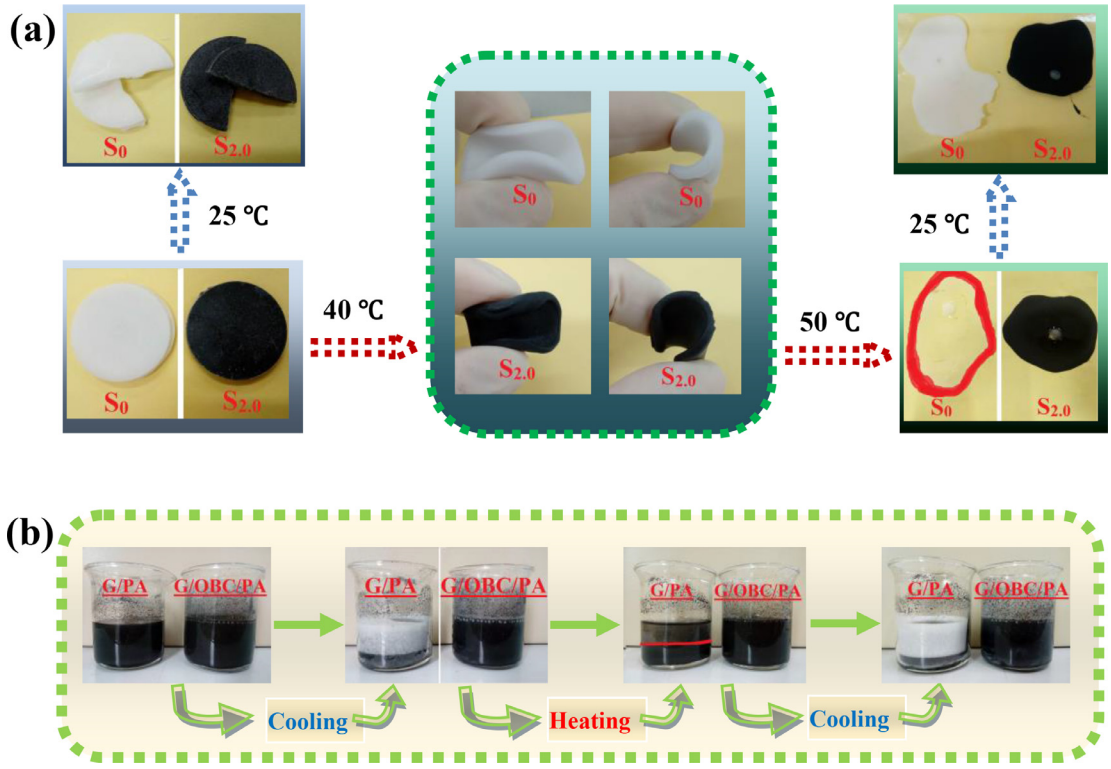

Fig. 4. Photographs of (a) temperature-dependent morphology of thermally induced elastic S_0 and $S_{2.0}$; (b) graphene is uniformly dispersed in the PA matrix.

2.3. Characterization

X-ray diffraction (XRD) with Cu Kα (λ= 0.154056 nm) was used to characterize the structure of the sample. The diffraction angle range was 5°–60° and the increase step was 0.02°. Scanning electron microscope (SEM) (FEI Sirion 200) was used to measure the morphology of graphene and the distribution of graphene in Ph-TIMs. Thermal conductivity meter (TCi-3-A, C-Therm Technologies Ltd., Canada) was used to test the thermal conductivity of Ph-TIMs. The interface thermal resistance measuring device (LW-9389, Long Win Science and Technology Corp.) was used for TCR analysis. The detailed measurement principle and data processing calculation can refer to the work that our research group has published (seen in supporting information S.1 and S.2) [29]. TCR and R_{TIMs} are calculated by the following formula:

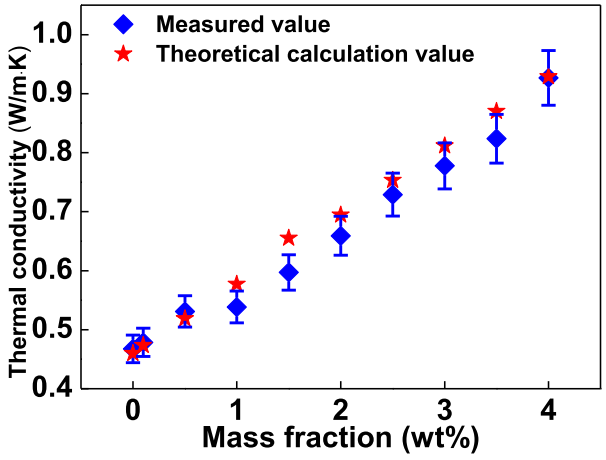

Fig. 5. Thermal conductivity of G/OBC/PA increases with the increase of mass fraction of graphene for experimental data and theoretical calculation values.

$$TCR1 + TCR2 = R_T - R_{TIMs} \quad (1)$$

$$R_{TIMs} = D/\lambda \quad (2)$$

Where R_T is total thermal resistance, $D$is the thickness of TIMs, and λ is the thermal conductivity of TIMs.

3. Results and discussion

Fig. 3(a) shows the SEM image of graphene. It is found that the two-dimensional thin-layer nanomaterials have the size of 20–50μm. Fig. 3(b) shows the dispersion of graphene in $S_{2.0}$ (other data see in supporting information S. 4). It can be seen that graphene is uniformly dispersed in the matrix, and the size of graphene is in the range of 20–50μm. Fig. 3(c) indicates the XRD result of graphene. A characteristic peak at 26.4° corresponds to the (220) crystal plane of graphene. Fig. 3(d) indicates the XRD results of S_0–$S_{4.0}$. For all the G/OBC/PA, it is found that there are characteristic peaks at 20.2°, 24.2°, 25.7° and 26.4°. Among them, the characteristic peak also appears at 26.4° corresponding to the (220) crystal plane of graphene. In addition, the characteristic peak appears at 20.2°, 24.2° and 25.7°, representing the crystallization of PA/OBC. These results confirm that the Ph-TIMs of G/OBC/PA have been successfully prepared.

Fig. 4(a) exhibits the temperature dependence of the thermally induced elasticity of the G/OBC/PA. At room temperature (25 °C), the G/OBC/PA is bent and found to be very easy to break. It proves that the G/OBC/PA shows strong brittleness. When the temperature increases gradually to 40 °C, the G/OBC/PA deforms in any shape and shows strong flexibility and elasticity. When the temperature rises further to 50 °C, the G/OBC/PA has completely transformed into molten state. Furthermore, the flexibility and elasticity can be restored again when the G/OBC/PA is cooled. These phenomena suggest that the G/OBC/PA can change from solid state to

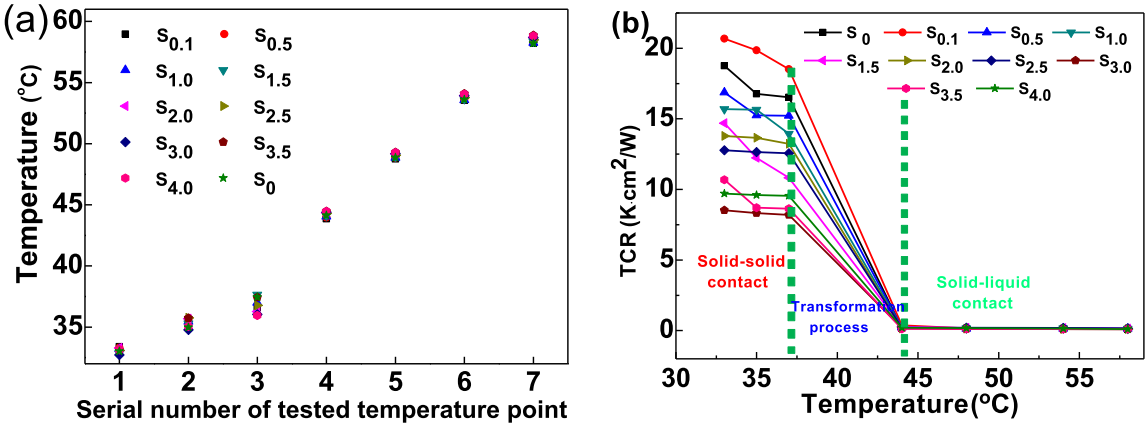

Fig. 6. Influence of temperature on the TCR of G/OBC/PA: (a) the obtained actual temperature value of each sample under different temperature control conditions; (b) TCR of G/OBC/PA changes with the temperature (50 Psi). The obtained actual temperature value is the average temperature of the hot end and the cold end of the Ph-TIMs during the thermal resistance test.

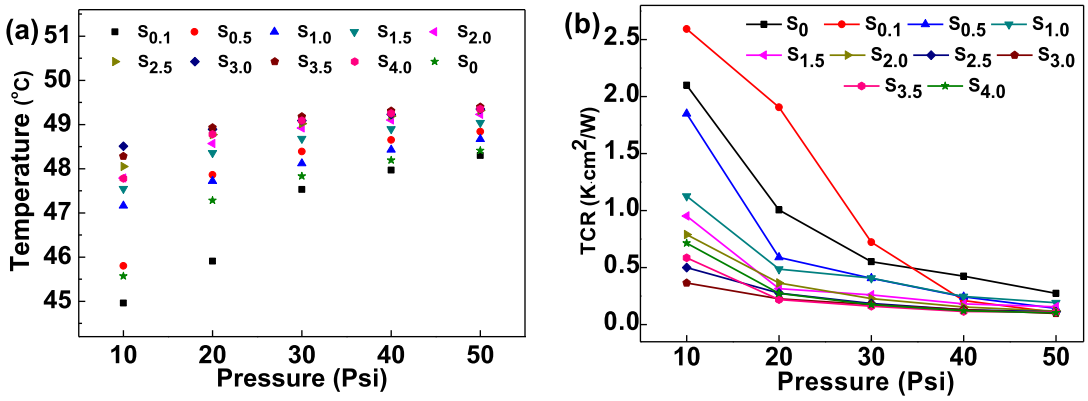

Fig. 7. Influence of pressure on the TCR of G/OBC/PA: (a) the obtained actual temperature value of each sample under different pressures and constant temperature; (b) TCR of G/OBC/PA changes with the pressure (48 °C).

molten state with the change of temperature. Meanwhile, there is little leakage for PA.

Fig. 4(b) is photograph for the dispersion of graphene in the matrix of G/PA (2.0 wt% graphene) and G/OBC/PA ($S_{2.0}$). In the initial stage, graphene is uniformly dispersed in PA and OBC/PA, respectively. After cooling, the G/PA is stratified, while the G/OBC/PA is still uniformly dispersed. After heating and cooling cycle again, the G/PA still appears stratification, and the G/OBC/PA is still in the state of uniform dispersion. These results confirm that the addition of OBC can effectively promote the even distribution of graphene in PA matrix.

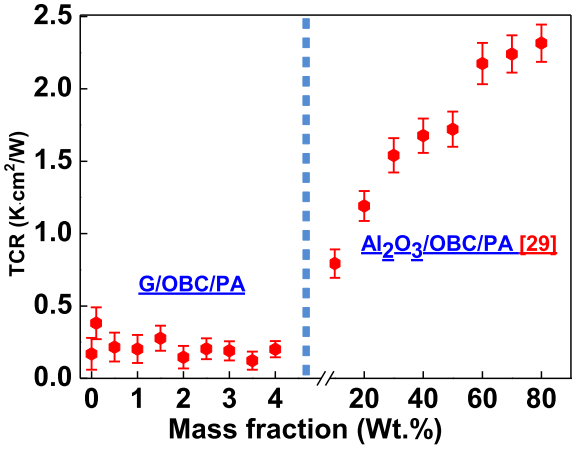

Fig. 8. Comparison of TCR of OBC/PA with filler at different mass fraction (44 °C, 50 Psi). The TCR value of Al_2O_3/OBC/PA is from reference 29.

3.1. Influence of temperature on the TCR of G/OBC/PA

Thermal conductivity of G/PA/OBC is an important factor for the heat dissipation process of microelectronic components. Fig. 5 shows the thermal conductivity of S_0–$S_{4.0}$. It is found that the thermal conductivity of PA/OBC is 0.467 W/mK, and those of PA/OBC filled with 0.1 wt% and 4.0 wt% graphene are 0.478 and 0.926 W/mK, respectively. The highest thermal conductivity ($S_{4.0}$) is enhanced up to 98.3% compared to pure PA/OBC (S_0). Furthermore, the thermal conductivity increases linearly with the increase of mass fraction of graphene. This is because the ratio of OBC to PA is fixed, which can be regarded as a uniform continuous phase with low thermal conductivity, while graphene is a dispersed phase with high thermal conductivity, so it meets the change of thermal conductivity of filled binary composite with low loading (Parallel Model).

TCR depends on the interaction of two direct contact surfaces. Temperature and pressure are the two most important factors affecting the interaction. The measurement process of TCR follows the steady-state heat conduction condition. Ph-TIMs is in the temperature gradient field, and the temperature value changes along the direction of heat flow. Therefore, the average temperature of the hot end and the cold end (the obtained actual temperature) is taken as the temperature of the Ph-TIMs. Fig. 6(a) shows the

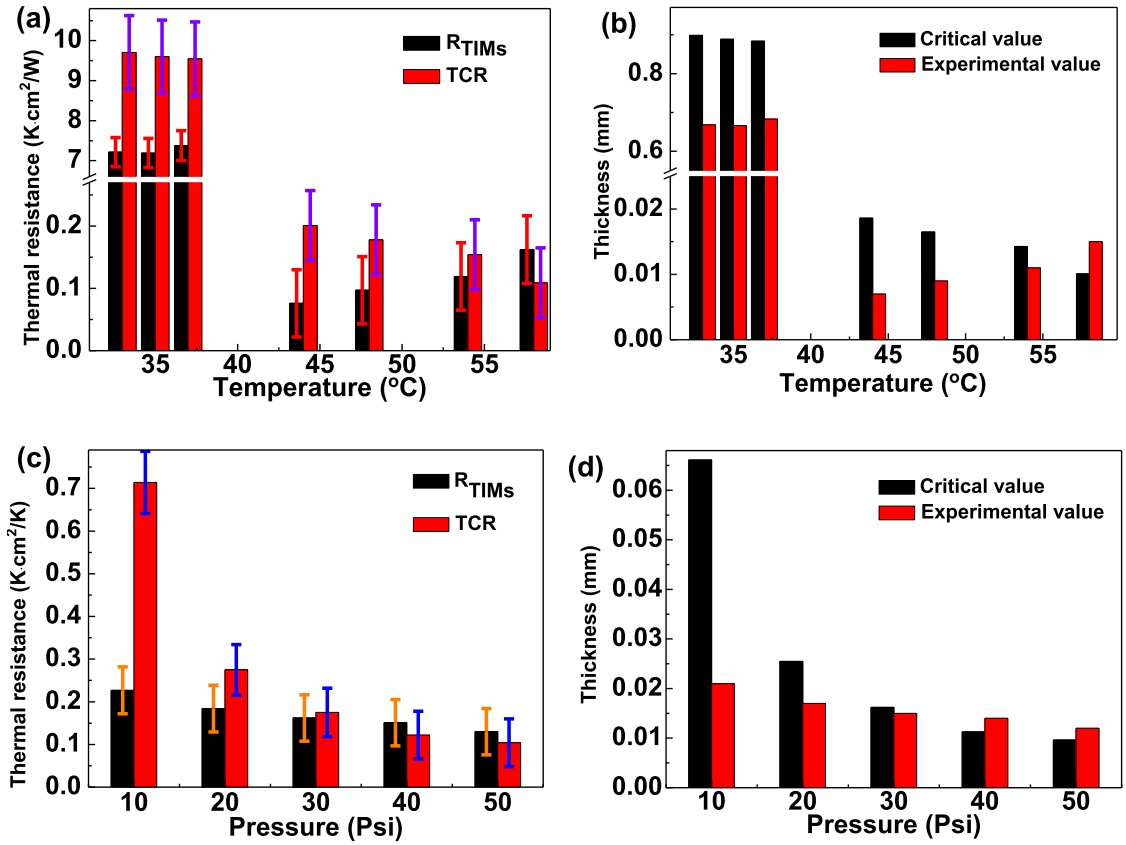

Fig. 9. Change of TCR and $R_{TIMs}$of $S_{4.0}$: (a) relationship between TCR or R_{TIMs} of $S_{4.0}$ and measured temperature (50 Psi); (b) experimental thickness and critical thickness of $S_{4.0}$ at different measured temperatures (50 Psi); (c) relationship between TCR or R_{TIMs} of $S_{4.0}$ and measured pressure (48 °C); (d) Experimental thickness and critical thickness of $S_{4.0}$ at different measured pressure (48 °C). Critical value is the thickness of $S_{4.0}$ when the R_{TIMs} is equal to the TCR.

obtained actual temperature distribution of all G/OBC/PA (S_0–$S_{4.0}$) under different temperature control conditions. It can be seen that all temperatures are concentrated near seven temperature points, such as 33 °C, 35 °C, 37 °C, 44 °C, 48 °C, 54 °C and 58 °C.

Fig. 6(b) shows the change of TCR of G/OBC/PA with temperature (50 Psi). It is found that the TCR decreases with the increase of temperature for all G/OBC/PA (S_0–$S_{4.0}$). When the temperature increases from 37 °C to 45 °C, the TCR of all G/OBC/PA decreases sharply from 8–20 Kcm^2/W to 0.1–0.2 Kcm^2/W, with a drop of up to two orders of magnitude. This is due to the gradual transformation of PA from solid to liquid in this temperature range, which greatly improves the wettability between two contact surfaces. When the temperature in the range of 44–58 °C, the TCR of all G/OBC/PA is maintained between 0.1 and 0.2 Kcm^2/W, with very small change. This is because all the Ph-TIMs of G/OBC/PA are in molten state at this temperature range, which is solid–liquid contact. Meanwhile, a small amount of graphene (≤4.0 wt%) cannot change the solid–liquid contact. Moreover, the TCR of the G/OBC/PA is 8–20 Kcm^2/W in the temperature range of 33–37 °C, and it decreases with the increase of graphene loading. This is owning to the solid–solid contact of the Ph-TIMs of G/OBC/PA and the slight change of the solid–solid contact due to the small amount of graphene.

3.2. Influence of pressure on the TCR of G/OBC/PA

Fig. 7(a) shows the obtained actual temperature value of each sample under different pressures (10–50 Psi). It indicates that the actual temperature value of all G/OBC/PA (S_0–$S_{4.0}$) are at the range of 47–49 °C. In addition, it can be seen from the results in Fig. 6(b) that the temperature has little effect on the TCR in this temperature range (47–49 °C). Therefore, these results can be regarded as the equivalent values obtained at a fixed temperature (48 °C).

Fig. 7(b) shows the TCR of G/OBC/PA changes with the pressure (10–50 Psi) under constant temperature (48 °C). The TCR of all G/OBC/PA are relatively low, because they are in solid–liquid contact (48 °C). In addition, with the increase of pressure, contact becomes more and more perfect, resulting in the decrease of TCR.

3.3. Influence of the amount of additives on the TCR of OBC/PA

Fig. 8 shows the TCR of OBC/PA with graphene or Al_2O_3 at different mass fraction (44 °C, 50 Psi). Because the filling limit mass fraction of graphene is relatively low, the TCR of Al_2O_3/OBC/PA with higher mass fraction is cited as a reference value [29]. It is found that the TCR of G/OBC/PA is 0.1–0.2 Kcm^2/W at the loading of 0.1–4 wt%, while the TCR of Al_2O_3/OBC/PA is 1–2 Kcm^2/W at the loading of 10–80 wt%. The TCR of OBC/PA increases with the increase of solid additives. At the temperature of 44 °C, the PA is in the molten state. Filling more solid additives will increase its viscosity and further affect the wettability. These results suggest that the solid additives have an important effect on the TCR as well as the thermal conductivity of Ph-TIMs.

3.4. Comparison of TCR and $R_{TIMs}$of G/OBC/PA

Thermal resistance is used to evaluate the heat dissipation ability of the Ph-TIMs of G/OBC/PA. It includes two parts: TCR and R_{TIMs}. The TCR is mainly affected by the wettability between the two contact surfaces. However, the R_{TIMs} is mainly affected by the thermal conductivity and thickness of the G/OBC/PA, which can

Table 2
Critical thickness of $S_{4.0}$ at different temperature.

Temperature (°C)	33	35	37	44	48	54	58
TCR (Kcm^2/W)	9.706	9.598	9.544	0.201	0.178	0.154	0.109
Critical thickness (mm)	0.899	0.889	0.884	0.019	0.016	0.014	0.010
Experimental thickness (mm)	0.668	0.666	0.683	0.007	0.009	0.011	0.015

Table 3
Critical thickness of $S_{4.0}$ at different pressure.

Pressure (Psi)	10	20	30	40	50
TCR (Kcm^2/W)	0.714	0.275	0.175	0.122	0.104
Critical thickness (mm)	0.066	0.025	0.016	0.011	0.010
Experimental thickness (mm)	0.021	0.017	0.015	0.014	0.012

be calculated by formula 2. In general, there is a linear relationship between the R_{TIMs} of G/OBC/PA and thickness. In practical application, the thickness of G/OBC/PA will be as thin as possible. Here, critical thickness is defined, that is the thickness of G/OBC/PA when the R_{TIMs} is equal to the TCR. It can be calculated by formula 3. Moreover, it is proposed to quantitatively evaluate the leading role of TCR or R_{TIMs} in total thermal resistance.

$$D_c = TCR \times \lambda \tag{3}$$

Wherein, $D_c$is critical thickness, $\lambda$is the thermal conductivity of $S_{4.0}$, $\lambda = 0.926W/mK$.

$S_{4.0}$ is taken as the specific object to analyze the relationship between TCR and R_{TIMs}. Fig. 9(a) shows the TCR and R_{TIMs} of $S_{4.0}$ at the temperature range of 33–58 °C (50 Psi). Fig. 9(c) shows the TCR and R_{TIMs} of $S_{4.0}$ at the pressure range of 10–50 Psi (48 °C). Fig. 9(b) and Table 2 provide the experimental thickness and critical thickness of $S_{4.0}$ at different measured temperatures. Fig. 9(d) and Table 3 provide the experimental thickness and critical thickness of $S_{4.0}$ at different measured pressure. These results exhibit that there is no correlation between TCR and R_{TIMs}. However, the dominant position of TCR or R_{TIMs} in total thermal resistance can be quantitatively evaluated by using critical thickness. When the experimental thickness is larger than the critical thickness, the R_{TIMs} is dominant. It can improve the thermal transport properties of G/OBC/PA through various ways. On the contrary, when the experimental thickness is less than the critical thickness, the TCR is dominant. The TCR can be reduced by changing wettability of Ph-TIMs from solid–solid contact to solid–liquid contact. Certainly, more ways to reduce TCR are expected.

4. Conclusions

A Ph-TIMs of G/OBC/PA filled with a small amount of graphene (≤4.0 wt%) was prepared. The OBC can effectively promote the form-stability of PA and the even distribution of graphene in PA matrix. These results exhibit that when the temperature increases from 37 °C to 45 °C (50 Psi), the TCR of all G/OBC/PA decreases sharply from 8–20Kcm^2/W to 0.1–0.2 Kcm^2/W, with a drop of up to two orders of magnitude. This is because the contact changes from solid–solid contact to solid–liquid contact, which greatly improves the wettability between two contact surfaces. For the temperatures in the range of 44–58 °C (50 Psi), the TCR of all G/OBC/PA is maintained between 0.1 and 0.2 Kcm^2/W, with very small change. In addition, when the pressure is at the range of 10–50 Psi (48 °C), the TCR decreases slightly with the increase of pressure. Moreover, the addition of a small amount of graphene can significantly enhance the thermal conductivity of G/OBC/PA, but the effect on the TCR is relatively weak.

The Ph-TIMs of G/OBC/PA ($S_{4.0}$) is chosen as the object to analyze the change of TCR and R_{TIMs} in practical application. The critical thickness is proposed to quantitatively evaluate the dominant position of TCR or R_{TIMs} in total thermal resistance. When the experimental thickness is larger than the critical thickness, the R_{TIMs} is dominant. It can improve the thermal transport properties of G/OBC/PA through various ways. On the contrary, when the experimental thickness is less than the critical thickness, the TCR is dominant. The TCR can be reduced by changing contact of Ph-TIMs from solid–solid contact to solid–liquid contact. Furthermore, the working mechanism of Ph-TIMs is simply described.

Author statement

W. Yu, H. Xie and B. Cao designed the work and checked the manuscript. C. Liu and C. Chen performed the data analysis and wrote the paper. All authors wrote the paper and the author list is agreed by all authors.

Declaration of Competing Interest

There is no conflict of interest in this work.

Acknowledgments

This work was supported by National Natural Science Foundation of China (Grant No. 51590902 and 51876112), Hunan Provincial Natural Science Fund (2018JJ3478) and the Key projects of Hunan Provincial Education Department (no. 19A448).

Supplementary materials

Supplementary material associated with this article can be found, in the online version, at doi:10.1016/j.ijheatmasstransfer.2020.120393.

References

[1] D Jeon, S H Kim, W Choi, et al., An experimental study on the thermal performance of cellulose-graphene-based thermal interface materials, Int. J. Heat Mass Transf. 132 (2019) 944–951.
[2] C P Feng, L B Chen, G L Tian, et al., Multifunctional thermal management materials with excellent heat dissipation and generation capability for future electronics, ACS Appl. Mater. Interfaces 11 (20) (2019) 18739–18745.
[3] C Liu, M Chen, D Zhou, et al., Effect of filler shape on the thermal conductivity of thermal functional composites, J. Nanomater. (2017) 1–15.
[4] W Yu, C Liu, L Qiu, et al., Advanced thermal interface materials for thermal management, Eng. Sci. 2 (2018) 95–97.
[5] C Liu, M Chen, W Yu, et al., Recent advance on graphene in heat transfer enhancement of composites, ES Energy Environ. 2 (2018) 31–42.
[6] L Qiu, P Guo, H Zou, et al., Extremely low thermal conductivity of graphene nanoplatelets using nanoparticle decoration, ES Energy Environ. 2 (2018) 66–72.
[7] J W Zhao, R Zhao, Y K Huo, et al., Effects of surface roughness, temperature and pressure on interface thermal resistance of thermal interface materials, Int. J. Heat Mass Transf. 140 (2019) 705–716.
[8] T Liang, M Zhou, P Zhang, et al., Multilayer in-plane graphene/hexagonal boron nitride heterostructures: Insights into the interfacial thermal transport properties, Int. J. Heat Mass Transf. 151 (2020) 119395.
[9] B Feng, J Tu, Y H Zhang, et al., An improved steady-state method for measuring the thermal contact resistance and bulk thermal conductivity of thin-walled materials having a sub-millimeter thickness, Appl. Therm. Eng. (2020) 114931.
[10] I L Ngo, V A Truong, An investigation on effective thermal conductivity of hybrid-filler polymer composites under effects of random particle distribution, particle size and thermal contact resistance, Int. J. Heat Mass Transf. 144 (2019) 118605.

[11] J Wang, Z Zhang, R Shi, et al., Thermal contact resistance: impact of nanoscale roughness on heat transport across the solid–solid interface, Adv. Mater. Interfaces 7 (4) (2020) 2070018.
[12] M T Barako, S G Isaacson, F Lian, et al., Dense vertically aligned copper nanowire composites as high performance thermal interface materials, ACS Appl. Mater. Interfaces 9 (48) (2017) 42067–42074.
[13] Y F Zhang, D Han, Y H Zhao, et al., High-performance thermal interface materials consisting of vertically aligned graphene film and polymer, Carbon 109 (2016) 552–557.
[14] J Chen, X Huang, B Sun, et al., Vertically aligned and interconnected boron nitride nanosheets for advanced flexible nanocomposite thermal interface materials, ACS Appl. Mater. Interfaces 9 (36) (2017) 30909–30917.
[15] H Ye, B Han, H Chen, et al., The liquid-exfoliation of graphene assisted with hyperbranched polyethylene-g-polyhedral oligomeric silsesquioxane copolymer and its thermal property in polydimethylsiloxane nanocomposite, Nanotechnology 30 (35) (2019) 355602.
[16] C Liu, Y He, C Chen, et al., Synergistic enhancement of heat transfer between irregular shaped particles and boron nitride flakes at low loading, Resul. Phys. 15 (2019) 102599.
[17] C Liu, C Chen, H Wang, et al., Synergistic effect of irregular shaped particles and graphene on the thermal conductivity of epoxy composites, Polymer Composites 40 (S2) (2019) E1294–E1300.
[18] M Hao, Z Huang, K R Saviers, et al., Characterization of vertically oriented carbon nanotube arrays as high-temperature thermal interface materials, Int. J. Heat Mass Transf. 106 (2017) 1287–1293.
[19] Y Zhao, M Zheng, J Wu, et al., Studying thermal transport in suspended monolayer molybdenum disulfide prepared by a nano-manipulator-assisted transfer method, Nanotechnology (2020).
[20] D Suh, C M Moon, D Kim, et al., Ultrahigh thermal conductivity of interface materials by silver-functionalized carbon nanotube phonon conduits, Adv. Mater. 28 (33) (2016) 7220–7227.
[21] H Wang, A S Tazebay, G Yang, et al., Highly deformable thermal interface materials enabled by covalently-bonded carbon nanotubes, Carbon 106 (2016) 152–157.
[22] M A Peacock, C K Roy, M C Hamilton, et al., Characterization of transferred vertically aligned carbon nanotubes arrays as thermal interface materials, Int. J. Heat Mass Transf. 97 (2016) 94–100.
[23] H Zhan, Y Nie, Y Chen, et al., Thermal transport in 3D nanostructures, Adv. Funct. Mater. (2019) 1903841.
[24] S Chen, Y Cheng, G Zhang, et al., Anisotropic wetting characteristics of water droplets on phosphorene: roles of layer and defect engineering, J. Phys. Chem. C 122 (8) (2018) 4622–4627.
[25] Z Zhang, Y Ouyang, Y Cheng, et al., Size-dependent phononic thermal transport in low-dimensional nanomaterials, Phys. Rep. 860 (2020) 1–26.
[26] R S Abdulrahman, F A Ibrahim, S F Dakhil, Development of paraffin wax as phase change material based latent heat storage in heat exchanger, Appl. Therm. Eng. 150 (2019) 193–199.
[27] A A Mikhaylov, A G Medvedev, D A Grishanov, et al., Doubly coated, organic–inorganic paraffin phase change materials: zinc oxide coating of hermetically encapsulated paraffins, Adv. Mater. Interfaces 6 (12) (2019) 1900368.
[28] W Wu, W Wu, S Wang, Form-stable and thermally induced flexible composite phase change material for thermal energy storage and thermal management applications, Appl. Energy 236 (2019) 10–21.
[29] C Liu, C Chen, W Yu, et al., Thermal properties of a novel form-stable phase change thermal interface materials olefin block copolymer/paraffin filled with Al_2O_3, Int. J. Therm. Sci. 152 (2020) 106293.